Revista de Matemática: Teoría y Aplicaciones **30**(2): 215-227
CIMPA - UCR ISSN: 1409-2433(Print), 2215-3373(Online)
DOI: https://doi.org/10.15517/rmta.v30i2.50449

ON THE RELATIONSHIP BETWEEN EXPANSION ANGLE OF EARTH-DIRECTED CMES AND SOFT X-RAY EMISSION FROM THEIR RELATED FLARE

SOBRE LA RELACIÓN ENTRE EL ÁNGULO DE EXPANSIÓN DE CMES DIRECCIONADOS A LA TIERRA Y LA EMISIÓN DE RAYOS X BLANDOS DESDE SU DESTELLO INICIAL

CAROLINA SALAS-MATAMOROS [1] JESÚS SÁNCHEZ-GUEVARA [2]

Received: 31/03/2022; Accepted: 29/05/2023

[1] Universidad de Costa Rica, Centro de Investigaciones Espaciales (CINESPA), Montes de Oca, San Jose, Costa Rica. E-Mail: carolina.salas_mata@ucr.ac.cr
[2] Universidad de Costa Rica, Escuela de Matemáticas, Montes de Oca, San Jose, Costa Rica. E-Mail: jesus.sanchez_g@ucr.ac.cr

Abstract

In space weather, to study the impact of Earth-directed coronal mass ejections (CME) in our terrestrial environment, one of the most important parameters is the propagation speed of these disturbances. We present an improvement of the 3D CME Geometrical Propagation-Expansion Description (3D-CGPED) model developed in previous work to increase the sample that we can use in CME arrival time predictions. This 3D model estimates the arrival time of Earth-directed CMEs at Earth by including a 3D geometry for the CME propagation and expansion in interplanetary space. Since the 3D-CGPED model computes the expansion of the CME based on the radial distance of the CME front, only travel times for CMEs with well-defined shapes seen by coronographs can be estimated. In the present work, we found an empirical relationship between the expansion angle of CMEs with well-defined shapes and the start-to-peak SXR fluence of their associated flares. We applied this relationship in the 3D-CGPED model to obtain the expansion angle for 8 CMEs with an irregular shape. We found similar window errors in arrival time predictions compared to the previous work. This result allows us to complement the 3D-CGPED model to include not only regular shapes but also irregular ones for CMEs observed by coronographs in future works.

Keywords: sun; coronal mass ejections; CME's; solar flare; radio waves.

Resumen

En clima espacial, en el estudio de los efectos terrestres de las eyecciones de masa coronal (CME) dirigidas a la Tierra, uno de los parámetros más importantes es la rapidez de propagación de estas perturbaciones. En este artículo presentamos una mejora del modelo 3D CME Geometrical Propagation-Expansion Description (3D-CGPED) desarrollado en un trabajo anterior para aumentar la muestra que podemos usar en las predicciones de tiempo de llegada de las CMEs. Este modelo 3D estima el tiempo de llegada a la Tierra de las CMEs al incluir una geometría 3D para la propagación y expansión de la CME en el espacio interplanetario. Dado que el modelo 3D-CGPED calcula la expansión de las CMEs en función de la distancia radial del frente de una CME, solo se pueden estimar los tiempos de viaje para las CME con formas bien definidas vistas por los coronógrafos. En el presente trabajo encontramos una relación empírica entre el ángulo de expansión de las CMEs con formas bien definidas y la fluencia SXR de inicio a pico de sus destellos asociados. Aplicamos esta relación en el modelo 3D-CGPED para obtener el ángulo de expansión para 8 CMEs con forma irregular. Encontramos ventanas de errores similares en las predicciones de tiempo de llegada en comparación con el trabajo anterior. Este resultado nos permite complementar el modelo 3D-CGPED en trabajos futuros, para incluir no solo formas regulares sino también irregulares, de CMEs observadas por coronógrafos.

Palabras clave: sol; eyeccción de masa coronal; CME's; erupción solar; ondas de radio.

Mathematics Subject Classification: Primary 85-04; Secondary 85-A35

1 Introduction

Space weather studies the relationship between the solar activity and its impact in the interplanetary medium. For Earth's environment, one of the principal aims of space weather is to forecast the travel time of Earth-directed coronal mass ejections (CMEs) until they arrive to Earth, because these magnetic structures can reach the Earth and cause geomagnetic storms. CMEs are observed remotely by coronographs such as the *Large Angle and Spectrometric Coronograph experiment* (LASCO) [1] of the *Solar and Heliospheric Observatory* (SoHO) and the instruments on-board STEREO mission [6], and recently by the instruments of the Parker Solar Probe (PSP; [7]) and Solar Orbiter [12] missions. Based on observations and theoretical modeling, different techniques have been developed to get an advance warning of the arrival of these magnetic disturbances (e.g., [2], [8], [18], [20], [16], [10], [17], [19], [3], [11]).

One of the most relevant CME properties to be known to forecast the arrival of CMEs is the propagation speed. Even though spacecrafts allow us to obtain speed measurements, they are not always in a position where the angle with respect to the Sun-Earth line is convenient to provide CME observations with minimum projection effects. In [13] and [14],the authors obtained empirical relationships to estimate the CME initial propagation speed based on radiative proxies to be applied in an empirical propagation model [9] to obtain the CME arrival times at 1 AU. These estimations were improved in a recent work [15] by including a 3D geometrical model (3D-CGPED) in the arrival time prediction procedure.

Given that the 3D-CGPED model requires the distance of the CME front as an input to calculate the expansion angle of CMEs in the interplanetary space λ (wich will be defined in detail in the next section), and some CMEs present irregular shapes in coronographs (either because they are intrinsically irregular, or because of the viewing perspective), in the present study we pursue an empirical relationship to estimate λ based on Soft X-ray (SXR) emission from the associated flares. In section 2 we present an overview of the geometrical model 3D-CGPED developed in the recent work [15]. Section 3 shows the procedure to obtain the correlation between the CME's expansion angle in the interplanetary space and SXR start-to-peak fluence of the related flare. The application of this relationship to determine ICME arrival time at Earth is presented in section 4. Finally, the results and conclusions are shown in sections 5 and 6, respectively.

2 Review of the geometric model for CME propagation

In this section we present an overview of the 3D-CGPED described in detail in [15], which is used to describe CME propagation and expansion in the interplanetary space from CME speed estimated by using radiative proxies ([13] and [14]).

In the 3D-CGPED model, the CME's geometry is modeled by using a time-changing surface: the CME's front is an ellipsoid and the back of the CME is a paraboloid (see Figure 1), with a radial symmetry along a straight line which is determined by the flare source location at the solar surface.

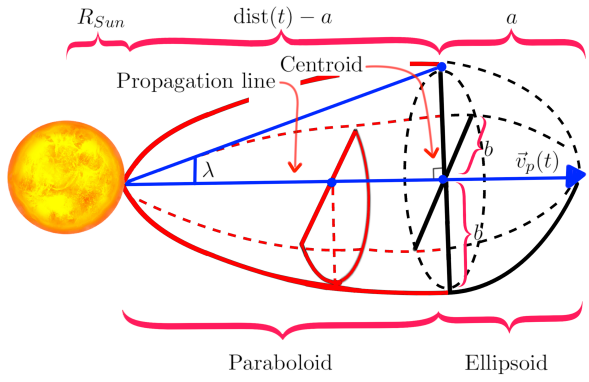

Figure 1: 3D-CGPED geometrical model representation. The CME's front is shown as the 3D surface in black and the 3D surface in red indicates the CME's back. The location of the centroid is indicated by a red arrow. The expansion angle λ is formed between the blue lines, one of them is the propagation line.

As the CME's flare source coordinates are at the solar surface, we obtain an unit vector $\vec{u}$, which defines a straight line through the Sun center. The CME'sfront moves along this straight line, which is given by the propagation vector

$$\vec{v}_p(t) = (R_{Sun} + \text{dist}(t))\vec{u},$$

where R_{Sun} is the solar radius and dist(t) is the distance to the CME's front from the solar surface at time t calculated following the procedure by [13] and [15].

In order to describe the surface that models the CME, we fix the time $t > 0$, and considered a positive real number $a < \text{dist}(t)$ such that the vector $C_t = \vec{v}_p(t) - a\vec{u}$ is placed between the solar surface and the CME's front.

From C_t to $\vec{v}_p(t)$ the surface behaves as an ellipsoid with centroid at C_t and radial symmetry along the propagation line. The ellipsoid semi-axe on the propagation line has length a. The other two semi-axes will have length b.

From C_t to the CME's flare source on the solar surface, the geometrical surface of the model is assumed to be a paraboloid with radial symmetry along the propagation line and the vertex at the CME's flare source. Both parts of the surface will intersect in the normal plane to $\vec{u}$ through C_t.

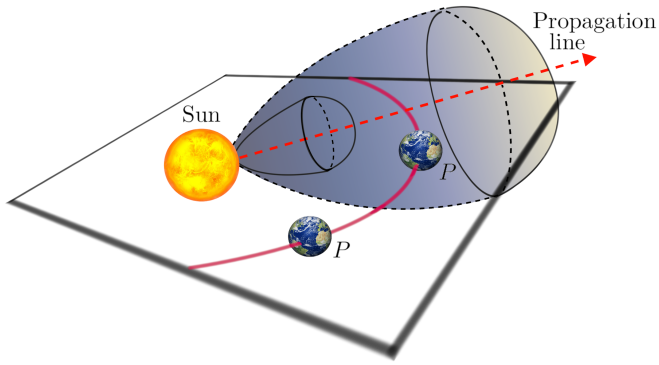

Figure 2: 3D-CGPED identification of the position of a point P. If Earth is at point P outside of the CME's surface then its coordinates in S_t satisfies that left side of equations 2.1 and 2.2 are > 1 and > 0, respectively. If P is inside the CME's surface, these numbers will be ≤ 1 or ≤ 0, respectively.

At C_t, we placed a new coordinate system $S_t = \vec{u}, \vec{v}, \vec{w})$. See [15] for the details about these unit vectors.

With S_t, the CME's surface is described at time t by the equations:

$$\frac{x_0^2}{a^2} + \frac{y_0^2 + z_0^2}{b^2} = 1, \quad x_0 \geq 0; \tag{2.1}$$

and

$$-\frac{x_0 + \text{dist}(t) - a}{\text{dist}(t) - a} + \frac{y_0^2 + z_0^2}{b^2} = 0, \quad x_0 \leq 0. \tag{2.2}$$

In the 3D-CGPED model, for each CME, a is assumed as half of the distance reached by the CME's front observed by coronographs.

On the other hand, b will be depending on time, it is given by

$$b = (\text{dist}(t) - a)\tan(\lambda),$$

where λ is called the expansion angle of the CME at the time it is first seen by coronographs. As it is explained in detail in [15], λ depends on the radial distance of the CME's front observed at that time. Because of that, only travel times for CMEs with a regular shape seen by coronographs can be estimated with this model.

Now we can determine, for any point in space P (see Figure 2), if it is inside the surface of the CME or not, at a specific time t by checking if the S_t

coordinates of P allow the equations for the ellipsoid or paraboloid, yield less than 1 or 0 (respectively).

Assuming that the Earth is located at P, the first t for which this relationship is satisfied indicates that the CME has arrived at Earth.

3 Correlation between CME expansion angle and soft X-ray fluence of the related flare

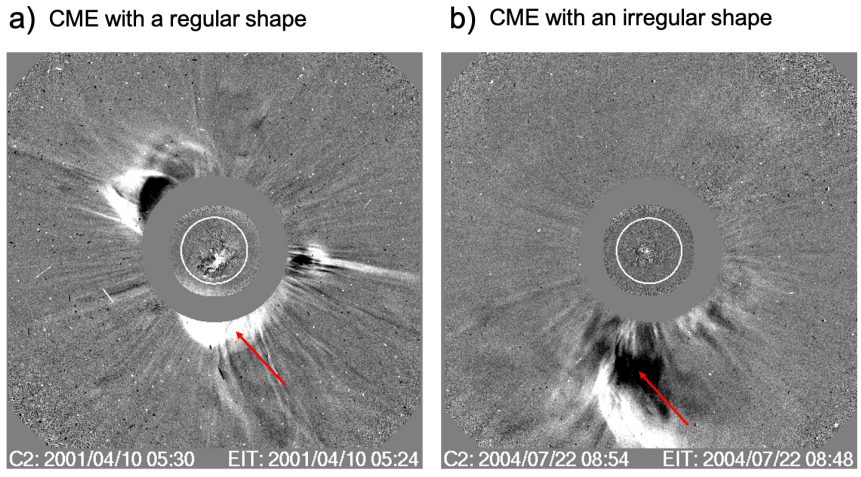

Figure 3: CME's front for two different CMEs: (a) CME with a regular shape and (b) CME with an irregular shape.

As was presented in the section above, the 3D-CGPED model uses not only the CME but also the associated flare parameters to determine the arrival time of the respective interplanetary coronal mass ejection (ICME) at Earth. This model applies CME parameters to estimate λ. Since one of the most important parameters is the radial distance of the CME's front at a certain time seen by coronographs, only CMEs with a regular shape (as it is shown in Figure 3.a) were taken into account. In our previous work, we found λ for 45 events listed in Table 1 in [15].

In the present study, we use the obtained data for those 45 events to correlate the expansion angle of CMEs and their respective start-to-peak fluences obtained from the soft X-ray flux data by the *Geostationary Operational Environmental Satellite* (GOES) satellite (see [4]) in the 0.1-0.8 nm channel.

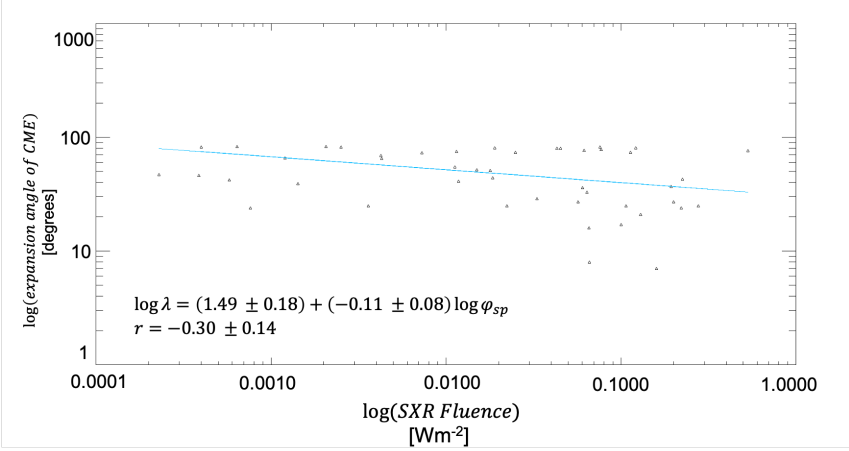

Figure 4: Logarithmic plot for λ and ϕ_{sp}. The solid line represents the linear fit obtained by the least squares (LS) method.

Figure 4 shows the scatter plot between the logarithm of the CME expansion angles at the moment of the LASCO first observation (λ) and the logarithm of the start-to-peak fluence of the Soft X-ray bursts of the associated flares (ϕ_{sp}) for these 45 events. A clear relationship between λ and the ϕ_{sp} is obtained as:

$$\log \lambda = (1.49 \pm 0.18) + (-0.11 \pm 0.08) \log \phi_{sp}. \tag{3.1}$$

We obtained a correlation of $r = -0.30 \pm 0.14$ and a statistically significant result of $p = 4.54$ x 10^{-13}. The value p is the probability of obtaining this or a higher correlation coefficient (r) from a random sample of uncorrelated events. The errors were calculated using a bootstrap method, where the correlation coefficient was calculated repeatedly a 1000 times for a random sample and, the mean and standard deviation are quoted as the correlation coefficient and its statistical uncertainty.

To find the statistical relationship between λ and ϕ_{sp}, we use least squares (LS) linear fit method to determine a straight line of the form which can be observed in light blue in Figure 4. This fit describes well the distribution of the sample, which clearly shows a trend to obtain lower values for λ as the fluence (ϕ_{sp}) increases. As a consequence, we can indicate that narrow CME expansion angles can be observed for CMEs with higher initial speed because the value of ϕ_{sp} is related with the initial propagation CME speed [13]. In the next section we apply this correlation, to be used in the propagation 3D-CGPED model to infer the arrival time at Earth.

4 Application of the relationship as an input in the 3D-CGPED model in ICME arrival at Earth

In this section we apply the relationship found in the section precedent to infer the expansion angle of CMEs based on the SXR bursts of the associated flares for irregular CMEs (see Figure 3.b) observed by the LASCO experiment ([1]) of the SoHO in the propagation 3D-CGPED model to infer the arrival time at Earth for a selected sample of 8 events. These 8 events listed in Table 1 (see in [15]) were discarded from the original sample because of their irregular shapes observed in the LASCO images. In this previous study, the data selection included criteria such as:

1. CME events with flare sources whose location were at solar latitudes between $-30°$ and $30°$, and heliolongitudes between $-65°$ and $65°$.
2. Clear identifiable soft X-ray flux profile measured by GOES in the 0.1–0.8 nm range.
3. Well defined CME-ICME pairs reported in the literature and verified by criterion of the drop in proton temperature by [5] in the data profile by the WIND spacecraft.
4. CMEs with a regular shape observed by the LASCO as is shown in Figure 3.a.

Table 1: Table of studied events: number of event (column 1), date (col. 2), LASCO CME onset (col. 3), coordinates of the associated flare (col. 4), start time of the SXR burst (col. 5), start-to-peak fluence of the SXR burst (col. 6), the value of λ infered by the relationship 3.1 (col. 7).

N	Date	LASCO CME	SXR parameters			Estimated
		onset	Coordinates	onset time	ϕ_{sp}	λ
		[UT]	[deg]	[UT]	[J m^{-2}]	[deg]
(1)	(2)	(3)	(4)	(5)	(6)	(7)
1	8 Jul 00	23:50	N18 W12	22:40	0.007479	53
2	7 May 02	04:25	S10 E25	03:30	0.003083	58
3	22 Jul 04	08:30	N04 E10	07:40	0.002524	60
4	14 Feb 11	18:24	S20 W17	17:20	0.001840	62
5	2 Sep 12	04:00	N04 W05	01:50	0.003945	57
6	13 Jan 13	12:00	N08 E04	11:14	0.007400	53
7	5 Jun 13	09:12	S28 W62	07:59	0.015358	49
8	2 Nov 13	04:48	S13 W14	04:41	0.000824	67

Since 3D-CGPED model requires the heliographic distance of the CME's front observed by coronographs at one specific time (RS), which is the first sight of the CME by the LASCO, some events were discarded. Inasmuch as the irregular shape of CMEs is common, especially for Earth-directed CMEs, in the present work we want to explore the possibility of using the relationship in Equation 3.1 as an input in the 3D-CGPED model for discarded events due to an irregular shape of the CMEs structure observed by the LASCO.

Table 1 contains the parameters of our studied sample of 8 events with these features. This table includes the parameters for coronographic observation of the CMEs (cols. 2-3), parameters of the related flare including the start-to-peak fluence of the SXR burst (cols. 4-6). Additionally, we calculated individually, the value of the expansion angle of the CMEs at the time of first sight by coronographs (λ) by using Equation 3.1. Those values are listed in column 7.

The obtained results in travel time predictions are presented in the next section.

5 Results

We have found estimations for the arrival time of time of the 8 studied events by using their parameters listed in Table 1. Consequently, Table 2 contains the arrival parameters for their correspondent ICMEs. This table displays the date and onset time of the ICME arrival detected by the WIND spacecraft and verified by the drop in proton temperature criterion [5] (cols. 2-3) and the predicted ICME arrival by using the 3D-CGPED model (cols. 4-5).

Table 2: Table of studied events: number of event (column 1), date of the ICME detection (col. 2), onset time of the ICME (col. 3), date of ICME arrival prediction (col. 4) and onset time of the ICME arrival prediction (col. 5).

N	Observed ICME arrival		ICME predicted arrival	
	Date	onset time [UT]	Date	onset time [UT]
(1)	(2)	(3)	(4)	(5)
1	11 Jul 00	22:30	12 Jul 00	15:24
2	11 May 02	15:55	10 May 02	17:56
3	24 Jul 04	17:30	26 Jul 04	03:30
4	18 Feb 11	04:48	18 Feb 11	13:12
5	4 Sep 12	21:57	6 Sep 12	21:45
6	16 Jan 13	10:38	16 Jan 13	23:44
7	6 Jun 13	15:00	5 Jun 13	07:00
8	7 Nov 13	09:14	6 Nov 13	12:02

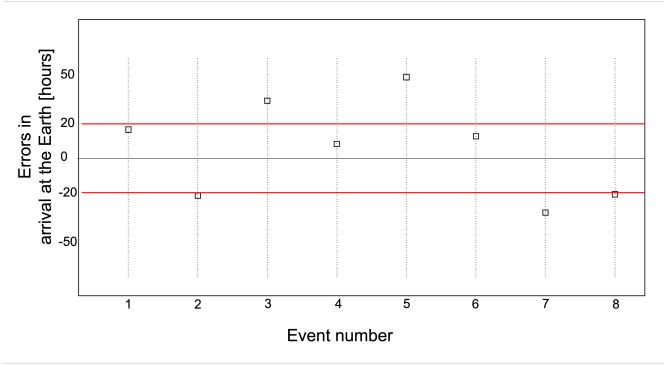

Figure 5: Predictions on arrival time at Earth respect to the observations of the ICME arrival at the WIND spacecraft. The horizontal black line at 0 corresponds to que ICME observed arrival time. The two red lines represent the range between -20 and 20 hours difference. The predictions are marked by black squares.

The difference in time between the observed and predicted arrival times is shown in Figure 5. The numbers in the x-axis refer to the number of event in Tables 1 and 2, while the y-axis contains the travel time errors with respect to the observations (black line at 0 hours in the Figure 5).

We observe that 5 events perform between the ±20 hours window. Also, 3 events show an underestimation of the travel time: 2, 7 and 8 with an error of −21.15 h, −32 h and −21.2 h respectively. Nevertheless, from the coordinates of the associated flares in Table 1, we did not find a correlation with the location of the associated flare. This is consistent with the result found previously in [15]. This is consistent with the result found previously for SXR emission proxy (see [13]). In previous work, the microwave emission associated to flares was also used as a proxy (see[14]). Then, to explore if the trend found here is also observed when a microwave proxy is used, a sample associated to microwave emissions should be studied in a future work.

Also, we calculated the mean errors which are included in Table 3. Compared with the previous work, we found a similar accuracy. Even though, our sample in this study is smaller compared to the sample of events in [15], this result indicates that the relationship for the estimation of λ can be used successfully when the CME shows an irregular shape in coronographs.

Additionally, in Figure 5 we notice that Event 5 shows the higher overestimation in the arrival time (+47.8 h), while Event 7 presents the higher underestimation in the predictions (-32 h). Regarding the initial speed for these two CMEs, we noticed that Event 7 is associated to the higher speed and Event 5 with the slower CME speed. Since 3D-CGPED model uses as an input the CME's initial speed estimated by using radiative proxies [13] and [14], this result indicates that it

could be associated with the partitioning of energy during the development of the associated flare. This confirms the result found in the previous work found in [15] where differences between estimations of arrival time by using different radiative proxies were found. This could be explained by the energy partitioning during the flare development.

Table 3: Average differences between estimations and observations of ICME arrival at Earth.

Proxy	Mean error [h]	Mean absolute error [h]
(1)	(2)	(3)
3D-CGPED model with Equation 3.1	5.6	24.4

6 Conclusions

In this work, we have found an empirical relationship between the expansion angle of Earth-directed CMEs (λ) in the interplanetary space and the SXR fluence of their associated flares. We have used only CMEs with regular shape seen by the LASCO and we found a negative correlation. Since the start-to-peak fluence is directly related with the initial CME propagation speed (see in [14]), a negative slope in the dispersion plot means that the angle λ decreases with higher initial CME propagation speeds. Considering that the 3D-CGPED model calculates λ from the high value of the CME's front in coronographic images, a more regular shape of the CME's front is required. Nevertheless, in some cases, CME's fronts can show extreme irregular shapes. In those cases, the relationship found in this study can be implemented in the 3D-CGPED model for ICME arrival time predictions. Our results showed that the accuracy was similar to previous work which demostrates that 3D-CGPED model can be implemented for both types of Earth-directed CMEs: with regular and irregular shapes observed by coronographs.

Finally, we found that two events with the higher and lower initial propagation speed were associated with an underestimation of the arrival time predictions. We want to explore in future work if the same trend is observed by using microwave emissions instead of SXR emissions or if the prediction improves. This future work will help us to have a better understanding of the energy partitioning that is potentially playing a role during flare development.

Acknowledgements and financial support

This study made extensive use of the CME catalogue, generated and maintained at the CDAW Data Center by NASA and The Catholic University of America in cooperation with the Naval Research Laboratory. SOHO is a project of international cooperation between ESA and NASA. GOES data were provided by NOAA

and the Solar Data Analysis Center (SDAC) at NASA Goddard Space Flight Center. The data bases of WIND were also used. We would also like to thank graphic designer Nayara Ureña Sánchez for her help with Figures 1 and 2. The authors acknowledges the financial support from Vicerrectoría de Investigación, Universidad de Costa Rica, through the projects C0072 and 821-B6-A19. The authors are grateful to the referees for their careful reading of the paper and helpful comments.

References

[1] G. E. Brueckner et al., *The Large Angle Spectroscopic Coronagraph (LASCO).* Solar Physics **162**(Dec. 1995), 357–402. DOI: 10.1007/BF00733434

[2] G. E. Brueckner et al., *Geomagnetic storms caused by coronal mass ejections (CMEs): March 1996 through June 1997.* Geophysical Research Letters **25**(Jan. 1998), no. 15, 3019–3022. DOI: 10.1029/98GL00704

[3] R. C. Colaninno, A. Vourlidas, C. C. Wu, *Quantitative comparison of methods for predicting the arrival of coronal mass ejections at Earth based on multiview imaging.* Journal of Geophysical Research (Space Physics) **118**(Nov. 2013), 6866–6879. DOI: 10.1002/2013JA019205

[4] J. M. Darnel et al., *The GOES-R Solar UltraViolet Imager.* Space Weather **20**(Apr. 2022), no. 4, e2022SW003044. DOI: 10.1029/2022SW003044

[5] H. A. Elliott et al., *An improved expected temperature formula for identifying interplanetary coronal mass ejections.* Journal of Geophysical Research (Space Physics) **110**(Apr. 2005), A04103. DOI: 10.1029/2004JA010794

[6] C. J. Eyles et al., *The Heliospheric Imagers Onboard the STEREO Mission.* Solar Physics **254**(Feb. 2009), no. 2, 387–445. DOI: 10.1007/s11207-008-9299-0

[7] N. J. Fox et al., *The Solar Probe Plus Mission: Humanity's First Visit to Our Star.* Space Science Reviews **204**(Dec. 2016), no. 1-4, 7–48. DOI: 10.1007/s11214-015-0211-6

[8] N. Gopalswamy, A. Lara, M. L. Kaiser, *An empirical model to predict the arrival of CMEs at 1 AU.* AAS/Solar Physics Division Meeting #31. 2000. Vol. 32. Bulletin of the American Astronomical Society, 825.

[9] N. Gopalswamy et al., *Predicting the 1-AU arrival times of coronal mass ejections.* Journal of Geophysical Research (Space Physics) **106**(2001), 29207–29218. DOI: 10.1029/2001JA000177

[10] P. K. Manoharan, *Evolution of Coronal Mass Ejections in the Inner Heliosphere: A Study Using White-Light and Scintillation Images.* Solar Physics **235**(May 2006), no. 1-2, 345–368. DOI: 10.1007/s11207-006-0100-y

[11] C. Möstl et al., *Connecting speeds, directions and arrival times of 22 coronal mass ejections from the Sun to 1 AU.* The Astrophysical Journal **787**(June 2014), 119. DOI: 10.1088/0004-637X/787/2/119

[12] D. Müller et al., *The Solar Orbiter mission*. Astronomy & Astrophysics **642**(Sept. 2020), A1. DOI: 10.1051/0004-6361/202038467

[13] C. Salas-Matamoros, K. Klein, *On the Statistical Relationship Between CME Speed and Soft X-Ray Flux and Fluence of the Associated Flare*. Solar Physics **290**(May 2015), no. 5, 1337–1353. DOI: 10.1007/s11207-015-0677-0

[14] C. Salas-Matamoros, K. Klein, G. Trottet, *Microwave radio emission as a proxy of CME speed in ICME arrival predictions at 1 AU*. Journal of Space Weather and Space Climate (2016), submitted.

[15] C. Salas-Matamoros, J. Sanchez-Guevara, *A geometrical description for interplanetary propagation of Earth-directed CMEs based on radiative proxies*. Monthly Notices of the Royal Astronomical Society **504**(July 2021), no. 4, 5899–5906. DOI: 10.1093/mnras/stab1232

[16] R. Schwenn, A. dal Lago, E. Huttunen, W. D. Gonzalez, *The association of coronal mass ejections with their effects near the Earth*. Annales Geophysicae **23**(2005), 1033–1059. DOI: 10.5194/angeo-23-1033-2005

[17] W. B. Song, *An Analytical Model to Predict the Arrival Time of Interplanetary CMEs*. Solar Physics **261**(Feb. 2010), no. 2, 311–320. DOI: 10.1007/s11207-009-9486-7

[18] B. Vršnak, N. Gopalswamy, *Influence of the aerodynamic drag on the motion of interplanetary ejecta*. Journal of Geophysical Research (Space Physics) **107**(Feb. 2002), 1019. DOI: 10.1029/2001JA000120

[19] B. Vršnak et al., *Propagation of interplanetary coronal mass ejections: the drag-based model*. Solar Physics **285**(2013), 295–315. DOI: 10.1007/s11207-012-0035-4

[20] Y. M. Wang et al., *A statistical study on the geoeffectiveness of Earth-directed coronal mass ejections from March 1997 to December 2000*. Journal of Geophysical Research (Space Physics) **107**(Nov. 2002), no. A11, 1340. DOI: 10.1029/2002JA009244